Flow boiling of ethanol/water binary mixture in a square mini-channel

Applied Thermal Engineering 127 (2017) 1617–1626

Contents lists available at ScienceDirect

Applied Thermal Engineering

journal homepage: www.elsevier.com/locate/apthermeng

Research Paper

Flow boiling of ethanol/water binary mixture in a square mini-channel

Parthenopi Vasileiadou [a], Khellil Sefiane [a,b,*], Tassos G. Karayiannis [c], John R.E. Christy [a]

[a] School of Engineering, University of Edinburgh, The King's Buildings, Mayfield Road, Edinburgh EH9 3JL, UK
[b] Tianjin Key Lab of Refrigeration Technology, Tianjin University of Commerce, Tianjin City 300134, PR China
[c] College of Engineering, Design and Physical Sciences, Brunel University London, Uxbridge UB8 3PH, UK

ARTICLE INFO

Article history:
Received 2 November 2016
Revised 12 August 2017
Accepted 27 August 2017
Available online 30 August 2017

Keywords:
Flow boiling
Heat transfer
Mixtures
Micro-channels

ABSTRACT

Two-phase flow heat transfer was examined in a single 5 mm inner hydraulic diameter square channel in a vertical orientation. The channel uses a resistive coating to allow for transparent heating of the walls. Transparency of the heating enabled high speed visualization of the boiling phenomena at various heat and mass fluxes. The pressure is monitored at the inlet and outlet of the channel. Infra-red thermography is used to map the external wall temperature of the channel and the local heat transfer coefficient is estimated from the local wall temperature and the saturation temperature of the liquid.

Ethanol, deionized water and a 5% v/v ethanol/water mixture were used as working fluids. Three mass fluxes (0.33, 0.66 and 1.00 kg/m^2 s) were tested as well as three heat fluxes (2.8, 4.2 and 6.1 kW/m^2). Experiments were conducted in a controlled temperature environment, where the surrounding air was kept at 40 °C. The addition of ethanol into water (5% v/v ethanol/water mixture) was found to enhance heat transfer resulting in higher heat transfer coefficients than for either of its pure components.

1. Introduction

Two-phase flow heat transfer has been under significant investigation over the past few decades. It is well known that heat transfer with phase change can result in increased heat transfer coefficients compared to single-phase heat transfer. These higher heat transfer coefficients occur naturally in some heat exchangers – primarily condensers and evaporators – which are widely used in industry. Recently, however, studies have been carried out focusing on two-phase flow heat transfer in the microscale. It has been suggested that two-phase flow increases heat transfer efficiency in microscale systems, and that it could thus be expected to serve as a competent cooling mechanism, for example in the cooling of microelectronic devices. Progress in the last few decades in the electronics sector has created a requirement for increased cooling efficiencies. Moreover, Micro-Electro-Mechanical Systems (MEMS), micro chemical reactors and compact heat exchangers, as well as other micro systems would benefit from increased heat transfer in the microscale. Hence, two-phase flow heat transfer has received significant attention from the international scientific community with the identification of the controlling mechanisms at the microscale being the main objective.

As reported by various studies [1–7], several factors have been found to affect the heat transfer of micro-cooling systems and enhanced heat transfer rates can be achieved by varying these factors. The main factors recognised are: the hydraulic diameter of the channels used [1,2], their surface roughness [3], their geometry [4], as well as the mass flux and the heat flux applied to the system. Moreover, the working fluid itself was found to be a determining factor in the heat transfer capability of a micro-system. A significant portion of research had been focused on different refrigerants, water and organic fluids. The thermophysical properties of an operating fluid were suggested to be important factors in heat transfer, since at the microscale surface tension and capillary forces are believed to have significant influence on heat transfer [5]. Moreover, the latent heat of vaporisation and fluid viscosity are indicated to have a significant role in microscale flow boiling, according to Peng et al. [6] who suggest that liquids with higher liquid to vapour density ratio, greater thermal diffusion coefficients and larger latent heats require higher heat flux for the initiation of nucleation. After the onset of nucleation, liquids that have lower surface tension and lower latent heat of vaporisation contribute to higher heat transfer coefficients, as stated by Greco and Vanoli [7].

A number of decades ago, chlorofluorocarbon refrigerants were the fluids of choice for cooling purposes, due to their thermal properties and stable structures. However, the impact of the fluids on the environment has been identified and investigated in recent

* Corresponding author at: School of Engineering, University of Edinburgh, The King's Buildings, Mayfield Road, Edinburgh EH9 3FB, UK.
E-mail address: ksefiane@ed.ac.uk (K. Sefiane).

http://dx.doi.org/10.1016/j.applthermaleng.2017.08.126
1359-4311/

times and hence, replacement liquids with similar heat transfer efficiencies have been considered, including mixtures. Miscellaneous multi-component mixtures have been used as working fluids in studies in order to determine their potential for heat transfer in micro-scale systems compared to their pure components or other pure liquids. Water is one of the most commonly used operating fluids as it is easily accessible and also a component in many organic binary mixtures. Kaya et al. [8] used water and examined the effect of high mass flux on critical heat flux (CHF) in fluid boiling, observing that CHF increased with increasing mass flux. It was also observed that high heat removal rates could be achieved (more than 300 MW/m^2) by combining short heated tube length, high mass flux and small hydraulic diameter. Yu et al. [9] noticed as well that CHF quality was dependant on mass flux for water in a small tube (d_h = 2.98 mm). However, it was recognised that boiling heat transfer of water is essentially only a function of heat flux, but not mass flux in this study. This trend could potentially be translated as the domination of nucleate to convective heat transfer in small channels. Nevertheless, Kosar et al. [10] (channel d_h = 227 μm, with deionised water) pointed out that both nucleate and convective heat transfer mechanisms were dominant, depending on the mass and heat flux applied to the system. Sumith et al. [11] (water, d_h = 1.45 mm) suggested that liquid film evaporation was the predominant heat transfer mechanism.

Pool boiling of binary mixtures of water with each of 2-propanol and methanol was investigated by McGillis et al. [12] and the CHF achieved, when small additions of alcohol were made to pure water, was found to be significantly higher than that of pure water. Fu et al. [13] experimented using ethanol/water mixtures in a diverging microchannel with microcavities. They showed that two-phase flow heat transfer coefficient was strongly dependant on the composition of the mixture, as well as on the wall superheat. Moreover, they concluded that addition of ethanol into water significantly increased the CHF recorded, with the maximum CHF being achieved for a 0.1 ethanol mole fraction. More specifically, the CHF of a mixture of 10% ethanol in water was found to be 110% that of pure water, and 234% that of pure ethanol. This increase in CHF was considered to be a result of the Marangoni effect occurring due to the addition of ethanol.

Mixtures of water with ethanol, propanol and butanol were examined by Suzuki et al. [14] in a subcooled flow boiling system to determine the effect that the addition of an organic fluid into water would have on heat transfer. It was observed that the maximum heat flux of the system increased with the addition of the organic fluid and that no dry-out was recorded under these circumstances. The maximum heat flux was found to be about 10% higher for the 10 wt% ethanol/water mixture compared to that for pure water, as was the case for Fu et al. [13] above.

In this study, new aspects of flow boiling heat transfer will be examined for a 5% v/v ethanol/water mixture and for its pure components (ethanol, water). The heat transfer coefficients of the three fluids, as well as the pressure drop of the system will be determined in order to investigate the effect that the addition of ethanol in water has on heat transfer rates and its potential as an enhanced fluid. The flow patterns were also assessed to provide a complete view of the prevailing phenomena.

2. Experimental apparatus and procedure

2.1. Test section

In this study a square cross-section channel of 5 mm inner hydraulic diameter, orientated with its axis vertical, was used as the test section. The channel was manufactured from borosilicate glass and the outer surface was sputtered with tantalum, allowing the channel to become electrically conductive while remaining transparent. Thus, heat could be applied to the system using a power supply and at the same time the flow patterns within the channel could be monitored with the use of a high speed camera. The wall thickness of the channel was measured to be 0.7 mm and the test section heated length was 72 mm.

The working fluids used for the experiments were a 5% v/v ethanol/water mixture and its pure components: deionised water and ethanol. Hence, a comparison of the heat transfer of the mixture with the pure components were obtained.

2.2. Experimental setup

The experimental setup consisted of a syringe pump that supplied the liquid to the channel and a DC power supply that provided the necessary power to heat up the system, through a transparent resistive coating on the outside of the test chamber.

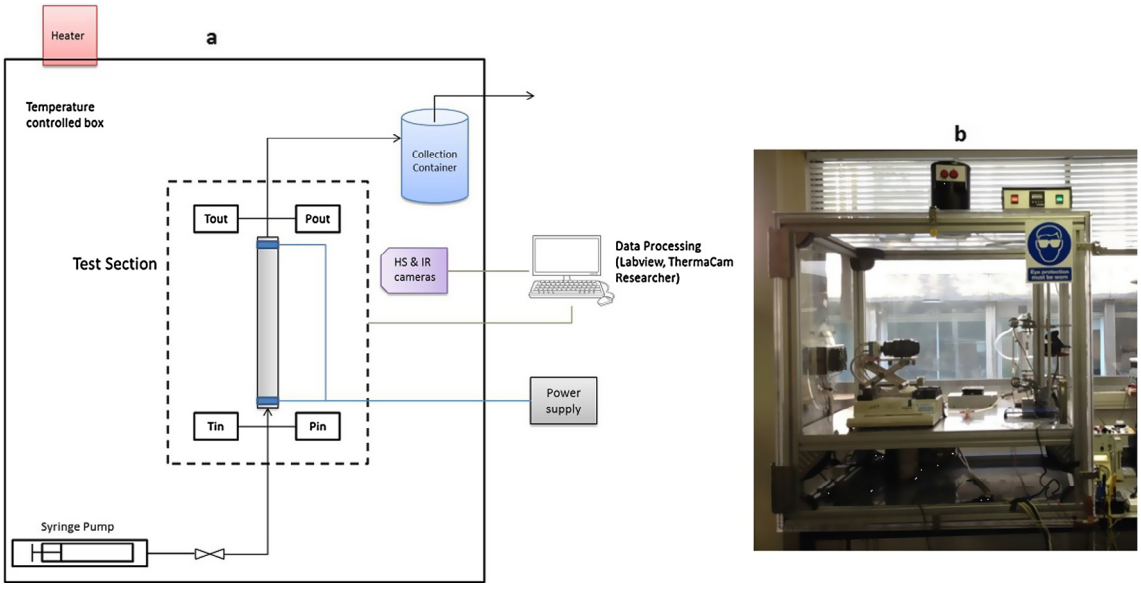

Fig. 1. Experimental setup (a) schematic diagram and (b) picture (showing the Plexiglas box with the equipment within).

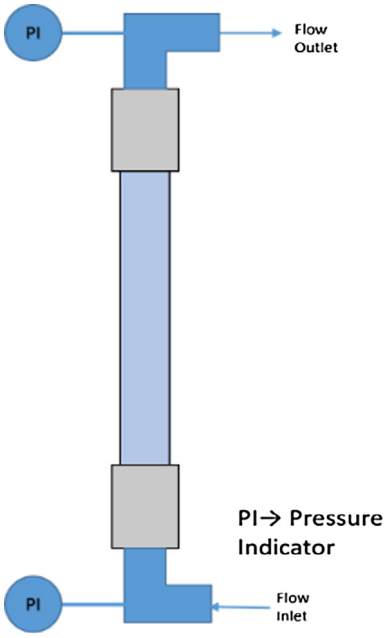

Fig. 2. Schematic diagram of pressure sensors positioning.

The experiments were conducted in a 1 m^3 (1 × 1 × 1 m^3) Plexiglas box which allowed for the control of the ambient temperature. The temperature was controlled by a PID controller mounted on the top of the Plexiglas box as depicted in Fig. 1, in order to ensure a constant temperature external to the test section.

The temperatures at the inlet and outlet of the channel were measured and recorded by two K-type thermocouples and the PID controller was connected with a third K-type thermocouple that was positioned inside the box. The pressure drop across the channel was also obtained during the experiments using two Omega PXM209 pressure transducers, positioned at the inlet and outlet of the channel (Fig. 2). The data were measured at a frequency of 6 Hz and recorded using National Instruments® software. A Mikrotron MC1310 high speed camera, set at 500 fps (frames per second), and a Thermovision® 900 infrared (IR) camera (at 6 fps) simultaneously recorded the growth and movement of vapour bubbles within the channel and the temperature profile of the outer channel wall. Experiments were conducted with three mass fluxes (0.33 kg/m^2 s, 0.66 kg/m^2 s and 1.00 kg/m^2 s) and three heat fluxes (2.8 kW/m^2, 4.2 kW/m^2 and 6.1 kW/m^2) for all three working fluids. The inlet temperature of the fluid was maintained constant at 40 °C, the same as the controlled environmental temperature, and at a pressure of 1 atm. Thus, the degree of subcooling for each fluid was different, being 60.0 °C for water, 38.4 °C for ethanol and 55.0 °C for the 5% v/v ethanol/water mixture.

3. Data reduction

Local heat transfer coefficients were obtained from the spatial temperature measurements at the wall and the local liquid saturation temperature by the following method.

3.1. Heat losses

The power (Q_{sup}) supplied to the system was computed using the voltage (V) and current (I) applied to the channel, using the equation:

$$Q_{sup} = VI. \quad (1)$$

For the experiments run with single-phase flow, the effective heat transferred to the liquid (Q_{eff}) was calculated as:

$$Q_{eff} = \dot{m} c_{P,L} (T_{out,avg} - T_{in,avg}) \quad (2)$$

where $\dot{m}$ is the mass flux (kg/s), $c_{P,L}$ is the specific heat capacity of the liquid (J/kg K), $T_{in,avg}$ and $T_{out,avg}$ are the inlet and outlet temperatures respectively (averaged over time).

The heat flux was then calculated as

$$q = Q_{eff}/A_{w,in} \quad (\mathrm{kW/m^2}) \quad (3)$$

where $A_{w,in}$ was the inner channel wall surface area (m^2).

For the cases where two-phase flow was present in the channel, the effective heat transfer to the fluid (Q_{eff}) was calculated from the heat supplied, Q_{sup}, minus the heat losses to the environment:

$$Q_{eff} = Q_{sup} - Q_{conv} - Q_{rad} \quad (4)$$

The heat loss was estimated taking into account the convective (Q_{conv}) and radiative (Q_{rad}) heat losses.

Convective heat loss was calculated by the following equation:

$$Q_{conv} = h_{conv} A_{w,out} (T_{w,avg} - T_{box}) \quad (5)$$

where h_{conv} is the convective heat transfer coefficient of air, which was estimated with the use of empirical correlations for natural convection; $A_{w,out}$ is the outer channel wall surface area; $T_{w,avg}$ is the average wall temperature over time and for the overall channel surface; and T_{box} is the temperature around the test section, hence the temperature in the Plexiglas box.

The radiative heat loss was then calculated from:

$$Q_{rad} = \varepsilon \sigma A_{w,out} (T_{w,avg}^4 - T_{box}^4) \quad (6)$$

where ε is the emissivity of the microchannel deposit and σ is the Stefan-Boltzmann constant (5.6703 × 10^{-8} W/m^2 K^4). The channel wall emissivity was experimentally estimated and fell into a range of 0.76–0.80. Hence an emissivity of 0.78 was used for the channel wall.

3.2. Heat transfer coefficient

Due to the limited field of view of the IR camera, infrared images of only the top 2.8 cm length of the channel were recorded and hence only the wall temperatures and local heat transfer coefficients for that region were obtained (the total length of the channel test section was 7.2 cm). The top part of the channel was chosen to be analysed since this is where boiling was expected to be present for all the cases where two-phase flow was achieved.

The Biot number (Bi) was calculated in an attempt to identify whether the temperature on the inside wall of the channel differs from the external surface temperature by comparing the conduction resistance to the convection resistance. The Biot number is:

$$Bi = \frac{h_c \delta_{wall}}{k_{glass}} \quad (7)$$

where h_c is the convective heat transfer coefficient, calculated from the Shah and London [15] correlation for fully developed laminar flow with uniform heat flux at the wall in a square channel, δ_{wall} is the channel thickness and k_{glass} is the channel thermal conductivity. The Biot number was calculated to be 0.035 and since $Bi \ll 1$, the difference between the inner and outer wall surface temperature may be assumed to be negligible. Thus, the outer channel wall temperature can be used to calculate the local heat transfer coefficient, h_w.

$$h_w = \frac{q_{eff}}{T_{w,local} - T_{sat}} \quad (8)$$

Table 1
Fluids' behaviour at different conditions.

$\acute{m}$ (kg/m^2·s)	Ethanol			Water			5% Ethanol/water		
	q (kW/m^2)								
	2.8	4.2	6.1	2.8	4.2	6.1	2.8	4.2	6.1
0.33	Two-phase	Two-phase	Two-phase	Single-phase	Two-phase	Two-phase	Two-phase	Two-phase	Two-phase
0.66	Two-phase	Two-phase	Two-phase	Single-phase	Two-phase	Two-phase	Single-phase	Two-phase	Two-phase
1.00	Two-phase	Two-phase	Two-phase	Single-phase	Single-phase	Two-phase	Single-phase	Single-phase	Two-phase

where $T_{w,local}$ is the local wall temperature and T_{sat} is the saturation temperature of the working fluid. This equation was used when two-phase flow was present in the channel (see Table 1 for when two-phase flow is present and this method is used). T_{sat} for the pure fluids was calculated as a function of temporal average inlet and outlet pressures and it was found that the saturation temperature only changed by 0.5 K (±1%) across the channel length. Hence, a constant saturation temperature was used for all the locations of the channel (average of inlet and outlet). For the 5% v/v ethanol/water mixture a similar behaviour was assumed, and a constant saturation temperature used, that was calculated from the vapour-liquid equilibrium data.

In **single-phase** flow cases the following equation was used to calculate the local heat transfer coefficients:

$$h_L = \frac{q_{eff}}{T_{w,local} - T_{l,local}} \tag{9}$$

where $T_{l,local}$ is the local liquid temperature.

The inlet and outlet fluid temperatures in this study were obtained by two thermocouples at the inlet and the outlet of the channel respectively. The local liquid temperature was calculated, assuming constant average heat flux and therefore a linear variation in temperature from the inlet to the outlet, as shown by the energy balance:

$$4zq_{eff} = c_p \acute{m} d_h (T_{l,local} - T_{in}) \tag{10}$$

where z is a local position along the channel, d_h is the inner hydraulic diameter of the channel, and T_{in} is the inlet liquid temperature. The local liquid temperature is therefore:

$$T_{l,local} = \frac{4q}{c_p \acute{m} d_h} z + T_{in} \tag{11}$$

Table 2
Experimental measurement and calculations uncertainties.

Parameter	Uncertainty (%)
Pressure	±0.2
Pump volumetric flow rate	±0.5
Voltage	±0.8
Current	±0.8
IR camera temperature	±1
Mass flux	±3
Heat flux	±7.3
Pressure drop	±0.5
Heat transfer coefficient	±20

$T_{w,local}$ is recorded using the IR camera.

3.3. Uncertainties

The experimental uncertainties arise primarily from equipment limitations. The main uncertainties were in the syringe pump velocity, the supplied power and the temperature measurements (mainly IR readings), that lead to uncertainties in the calculated values of mass and heat fluxes, as well as the heat transfer coefficients values. An uncertainty analysis was conducted and Table 2 summarises the results in percentage terms.

4. Results and discussion

4.1. High speed visualization results

In this set of experiments the liquid always entered subcooled at the bottom of the channel at the same inlet temperature (40 °C). Therefore, boiling only started further along the length of the channel and, since the subcooling and the properties of each fluid were different, the nucleation position was also different for each fluid for the same operating conditions (Table 3). The nucleation positions were determined by examining the high speed visual images obtained, with the use of imaging software (ImageJ).

Ethanol was found to be the fluid for which a lower amount of heat was required for the initiation of boiling, as was expected based on its properties. Moreover, it was observed that bubble nucleation was more easily initiated for the ethanol/water mixture than for pure water, suggesting that the addition of even a small amount (5% v/v) of alcohol in water was adequate to influence the properties of the mixture significantly. Boiling was also found to be more vigorous in the case of pure ethanol and the ethanol/water mixture. However, when mass flux was decreased and heat flux increased, dry-out was observed at the top of the channel, as can be seen in Fig. 3 for ethanol. Dry-out was also observed for water at 0.33 kg/m^2 s and 6.1 kW/m^2, but not for the mixture. The lack of dry-out for the mixture suggested a more reliable heat transfer system for cooling high heat flux components.

The boiling patterns observed varied depending on the operating conditions and the working fluid, but the main patterns recorded, as depicted in Fig. 4, were bubbly, slug and elongated slug/annular flow. These observations are in agreement with previous studies such as Huh and Kim [16] and Mishima and Hibiki [17]. Moreover, it was observed that in all cases a small bubble was

Table 3
Nucleation positions for all the fluids at the different operating conditions.

Nucleation position from entry [mm] (±0.5 mm)										
Working fluid	Mass flux [kg/m^2 s]	0.33			0.66			1.00		
	Heat flux [kW/m^2]	2.8	4.2	6.1	2.8	4.2	6.1	2.8	4.2	6.1
Ethanol		8.2	6.2	0	12.3	43.0	9.5	0	0	20.3
Water		n/a	53.5	39.0	n/a	52.0	53.4	n/a	n/a	60.7
5% Ethanol/water		47.0	19.5	47.1	n/a	53.0	47.0	n/a	n/a	45.0

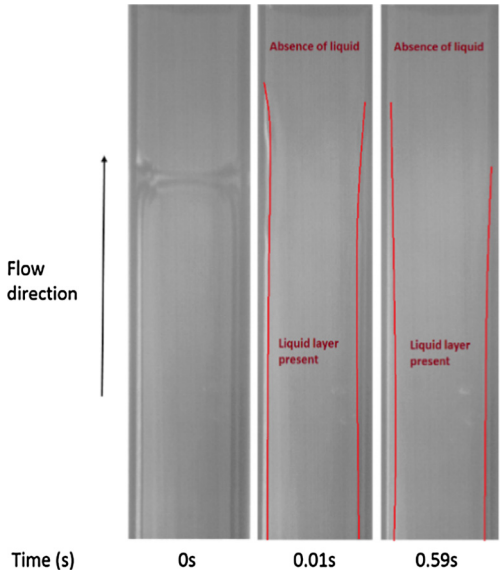

Fig. 3. Ethanol boiling at G = 0.33 kg/m^2 s and q = 6.1 kW/m^2, top 2.8 cm of the channel length is featured here.

initially formed that rapidly expanded into slug/annular flow. The sudden expansion of the vapour would lead to a momentary blockage or slowdown of liquid inflow and thus, to an increase in pressure drop. Liquid inflow was then restored and the channel was completely covered with liquid until the nucleation temperature was reached again. This repetitive bubble recoil, dewetting and rewetting, or ebullition cycle as referred to by Carey [18], is the mechanism that allows the heat of vaporisation of the liquid to be used as a heat transfer mechanism and possibly increase the heat transfer efficiency of two-phase flow compared to single-phase flow.

Finally, it was noticed that for an increased mass flux and constant heat flux, boiling would start further along the channel. In some cases, an increased heat flux was required for the commencement of nucleation (Fig. 5), which is in accordance with literature [19]. This phenomenon could be explained by the fact that a rise of mass flux would enhance convective heat transfer, dropping the wall temperature at a higher rate and hence, an increase in the heat supply would be needed to initiate bubble nucleation. On the other hand, increasing heat flux while keeping a constant mass flux would result in nucleation starting closer to the channel inlet since the increased fluid temperature would assist the activation of nucleation sites.

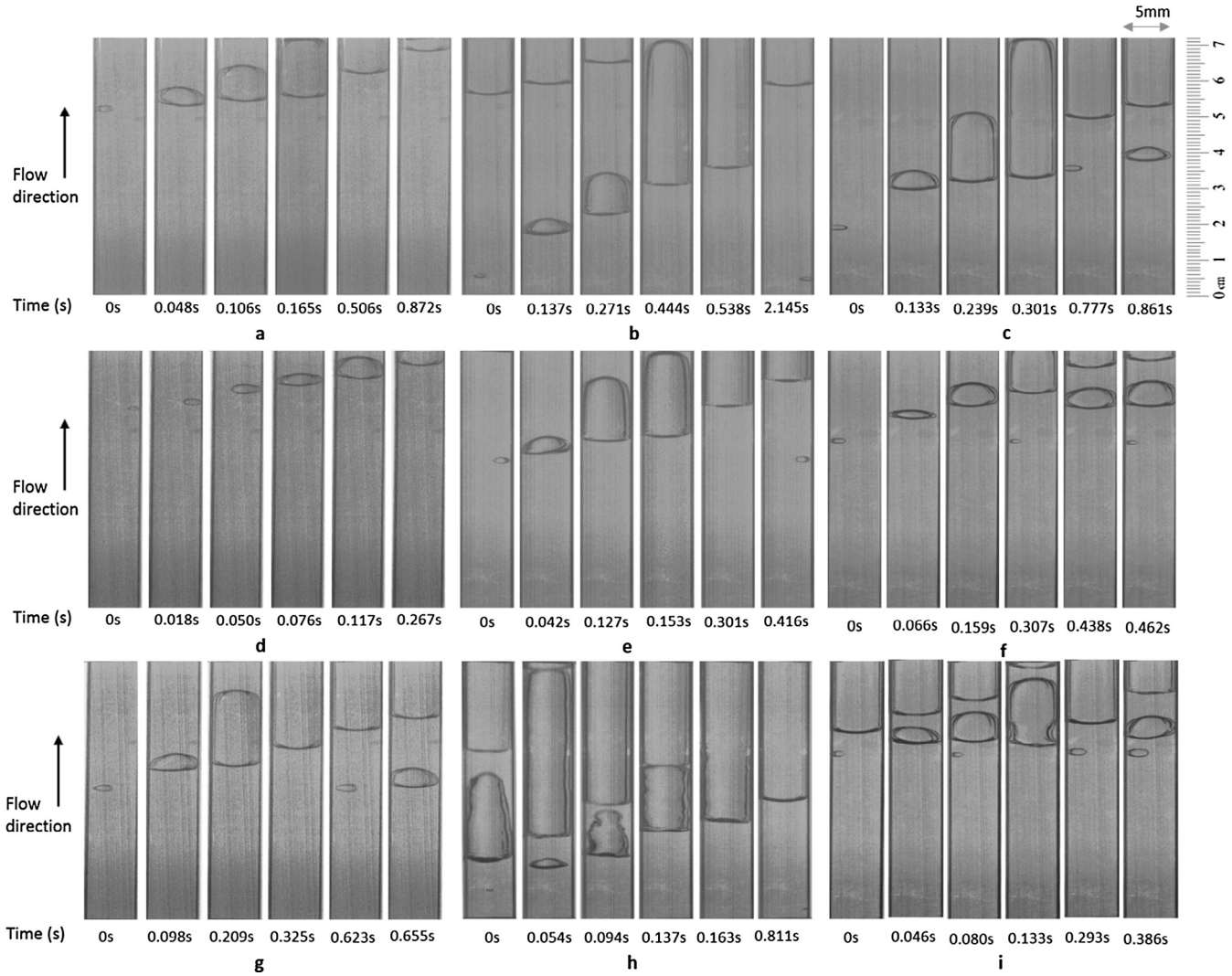

Fig. 4. Flow regimes of boiling at G = 0.33 kg/m^2 s and 4.2 kW/m^2 for (a) water, (b) ethanol and (c) 5% v/v ethanol/water mixture, at G = 0.66 kg/m^2 s and 4.2 kW/m^2 for (d) water, (e) ethanol and (f) 5% v/v ethanol/water mixture, and at G = 0.66 kg/m^2 s and 6.1 kW/m^2 for (g) water, (h) ethanol and (i) 5% v/v ethanol/water mixture, all the test section (7.2 cm) is featured here.

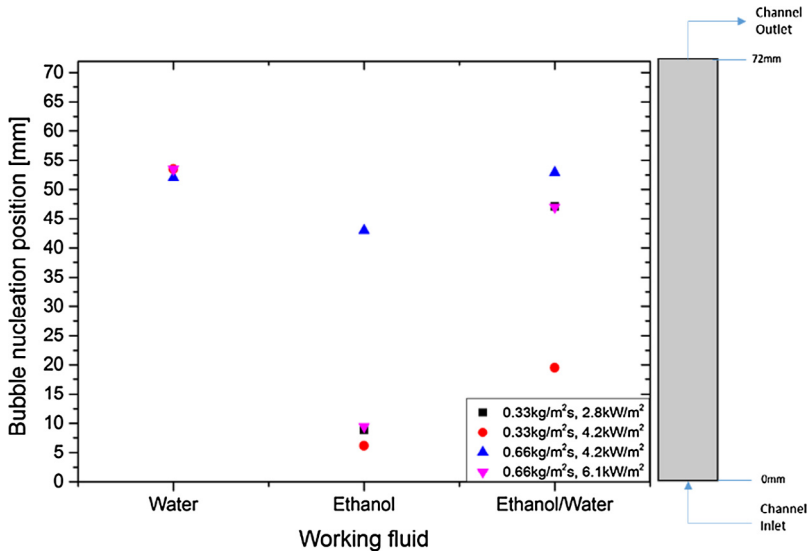

Fig. 5. Nucleation positions for all the fluids at different mass and heat fluxes.

4.2. Wall temperature fluctuations for the different fluids

The temperature profile of the top 2.8 cm of the channel outer wall was recorded with the IR camera at 6 fps Temperature fluctuations over time were observed, which are believed to be the result of boiling in the channel. Only part of the channel was thermally mapped due to the limited field of view and focal distance of the IR camera. The temperature data at the five positions ($T_{wall,L1}$, $T_{wall,L2}$, $T_{wall,L3}$, $T_{wall,L4}$ and $T_{wall,L5}$) shown in Fig. 6, were analysed.

From the experiments conducted, it was concluded that when the system is either single-phase or for positions upstream of boiling, the wall temperature was constant over time with no fluctuations present. On the other hand, during two-phase flow, wall temperature fluctuations were observed. Given that the heat was uniformly applied on the channel, it is assumed that these fluctuations were entirely a result of boiling. The aforementioned phenomena can be observed in Fig. 7, where until a certain length along the channel (x = 60.7 mm) there is no boiling present and hence there are no fluctuations in the wall temperature, while further along the channel the temperature starts fluctuating. Also, it could be implied that the fluctuations of the temperature were a result of the alternating boiling regimes within the channel (vapour occupying channel followed by rewetting). It was seen that the temperature increased when the channel was filled with vapour and it decreased when liquid was covering the heated channel wall again.

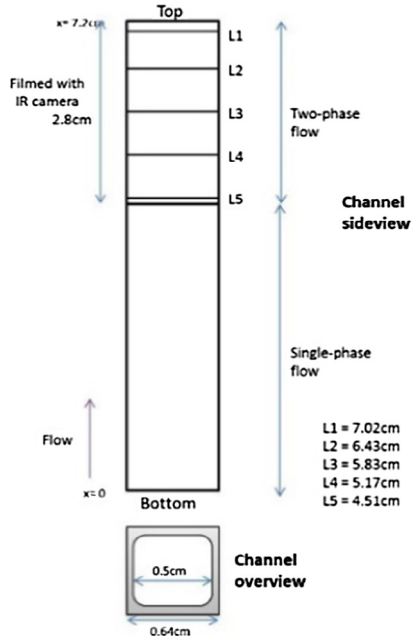

Fig. 6. Schematic diagram of the local heat transfer coefficients on the channel.

Comparing the wall temperature for the different fluids (Fig. 8), it can be seen that for the mixture the maximum temperature fluctuations were substantially smaller than those of either pure liquid.

Increasing the heat flux, while keeping a constant mass flux, tended to increase the amplitude of fluctuations for all the fluids. On the other hand, when mass flux was increased (at constant heat flux) it was evident that the amplitude of fluctuations reduced. Also, at experiments where two-phase flow was present, it was noticed that the wall temperature was lower further along the channel ($T_{wall,L1} < T_{wall,L5}$) which suggested that heat was removed at a higher rate, compared to single-phase flow, where the reverse observation was made ($T_{wall,L1} > T_{wall,L5}$) (Fig. 9). Finally, in the case of highest heat flux and lowest mass flux (6.1 kW/m^2, 0.33 kg/m^2 s) when ethanol and water were used as the working fluids, significant amplitude fluctuations in wall temperatures were observed (Fig. 9(2, 3)), which implies the presence of dry-out at the channel wall.

4.3. Pressure drop

The pressure drop across the length of the test section was also monitored in this study, in order to investigate the relationship between heat transfer and pressure effects. It was found that the pressure drop oscillated over time when boiling was present in the channel, and the magnitude and frequency of the fluctuations varied for different fluids and operating conditions. As was briefly explained in section 4.1, an increase in pressure drop was observed in the channel during bubble nucleation and especially when sudden vapour expansion occurred. The expansion of a bubble towards both the inlet and outlet caused a blockage of the liquid

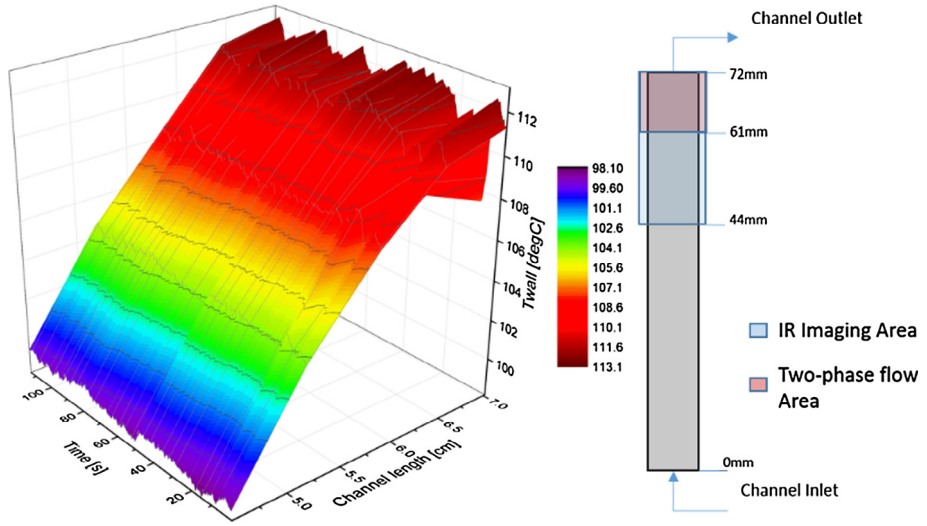

Fig. 7. A 3-dimensional plot of wall temperature against channel length of water at G = 1.00 kg/m^2 s, q = 6.1 kW/m^2.

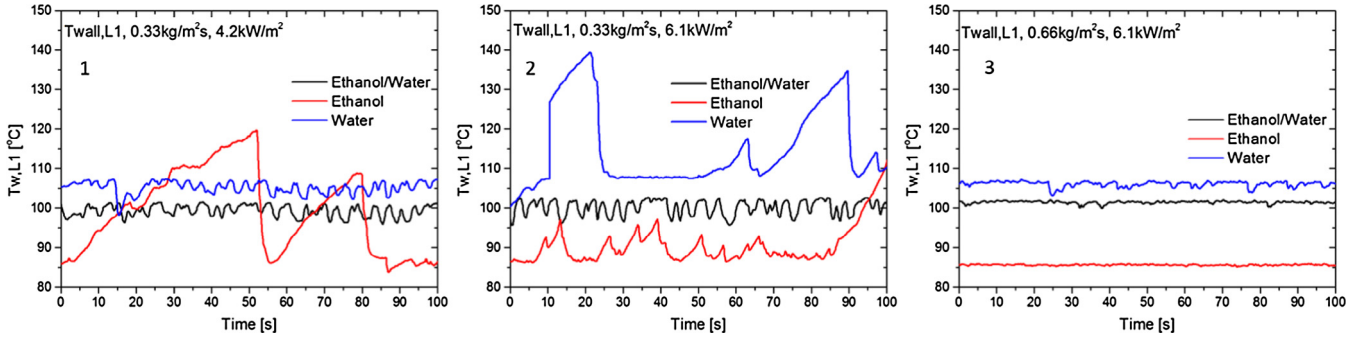

Fig. 8. Channel wall temperature fluctuation of the 5% v/v ethanol/water mixture, ethanol and water at (1) G = 0.33 kg/m^2 s, q = 4.2 kW/m^2, (2) G = 0.33 kg/m^2 s, 6.1 kW/m^2 and (3) G = 0.66 kg/m^2 s, q = 6.1 kW/m^2 at position channel position L1.

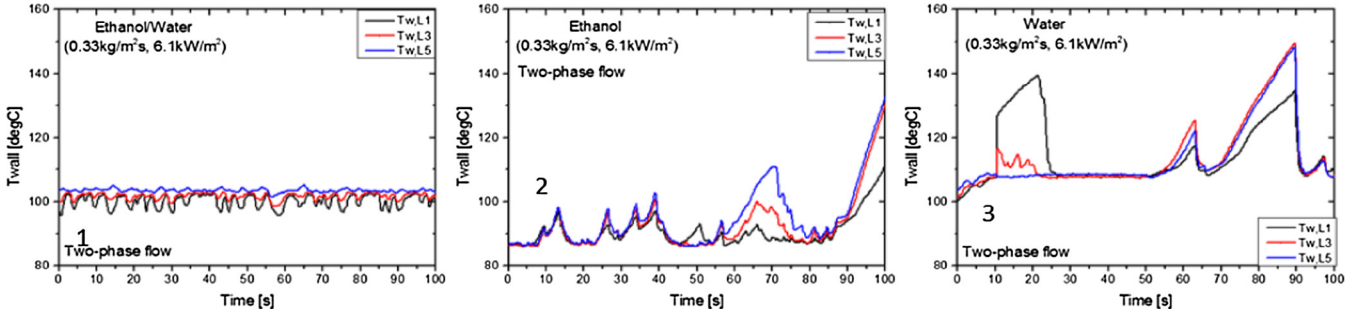

Fig. 9. Channel wall temperature fluctuation at G = 0.33 kg/m^2 s, q = 6.1 kW/m^2 for (1) ethanol/water, (2) ethanol and (3) water.

flow and led to the highest magnitude pressure drops, which were observed for mass and heat flux of 0.33 kg/m^2 s and 6.1 kW/m^2.

From Fig. 10, it can be seen that there are two type types of pressure drop fluctuations present: low amplitude, high frequency ones and high amplitude, low frequency ones. The second type of fluctuations is more evident in the cases of higher heat flux and smaller mass fluxes where boiling was more vigorous and the vapour expansion incidents were more violent. In Fig. 10 (1, 5 and 10) the thigh peaks in pressure drop due to the sudden expansion of vapour can be seen most clearly. The smaller amplitude oscillations are believed to be the result of bubble flow due to the movement and collisions of the bubbles.

4.4. Local heat transfer coefficients

Local heat transfer coefficients were calculated as a function of time for five positions in the upper section of the channel. Fig. 11 shows these plotted for position L1 against time for the three fluid at the nine combinations of heat flux and mass flux. For position L1, whenever the heat and mass flux led to boiling (Fig. 11(1, 2, 3, 5, 6, 9)), the heat transfer coefficient for the ethanol/water mixture generally exceeded that of either pure ethanol or pure water.

As expected, for all mass fluxes, increasing the heat flux resulted in increased heat transfer coefficients. Increasing the mass flux tended to lead to a decrease in the heat transfer coefficients,

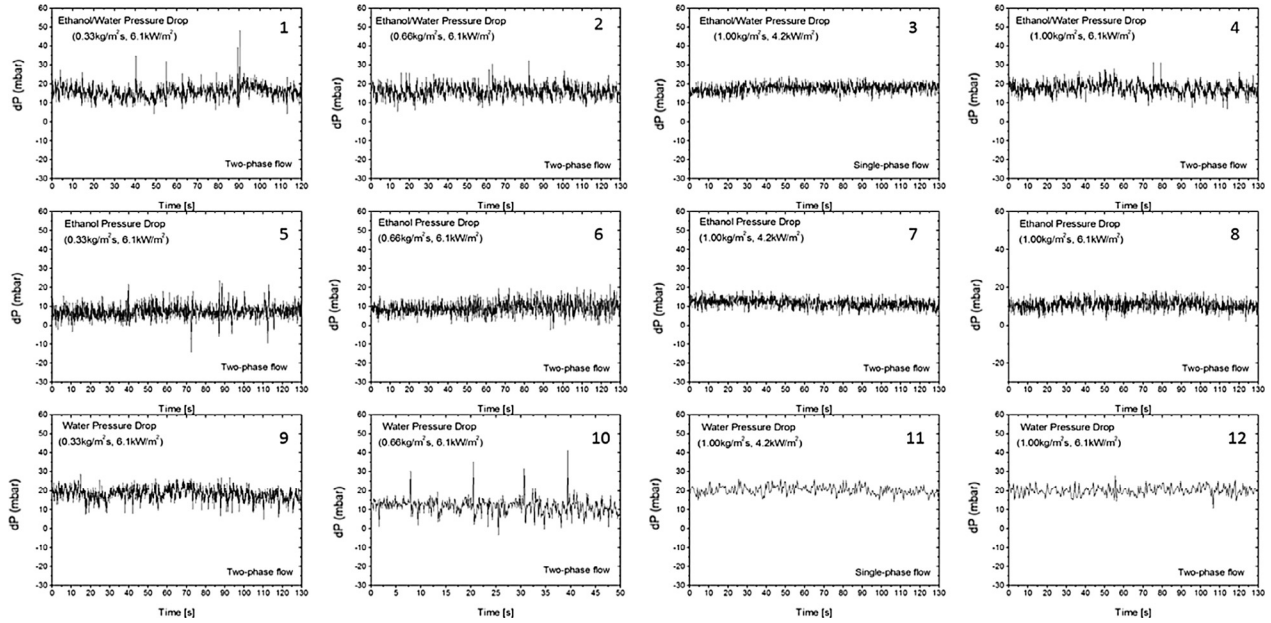

Fig. 10. Pressure drop along the channel for: 5% v/v ethanol/water mixture at (1) G = 0.33 kg/m^2 s, q = 6.1 kW/m^2, (2) G = 0.66 kg/m^2 s, q = 6.1 kW/m^2, (3) G = 1.00 kg/m^2 s, q = 4.2 kW/m^2 and (4) G = 1.00 kg/m^2 s, q = 6.1 kW/m^2 Ethanol at (5) G = 0.33 kg/m^2 s, q = 6.1 kW/m^2, (6) G = 0.66 kg/m^2 s, q = 6.1 kW/m^2, (7) G = 1.00 kg/m^2 s, q = 4.2 kW/m^2 and (8) G = 1.00 kg/m^2 s, q = 6.1 kW/m^2 Water at (9) G = 0.33 kg/m^2 s, q = 6.1 kW/m^2, (10) G = 0.66 kg/m^2 s, q = 6.1 kW/m^2, (11) G = 1.00 kg/m^2 s, q = 4.2 kW/m^2 and (12) G = 1.00 kg/m^2 s, q = 6.1 kW/m^2.

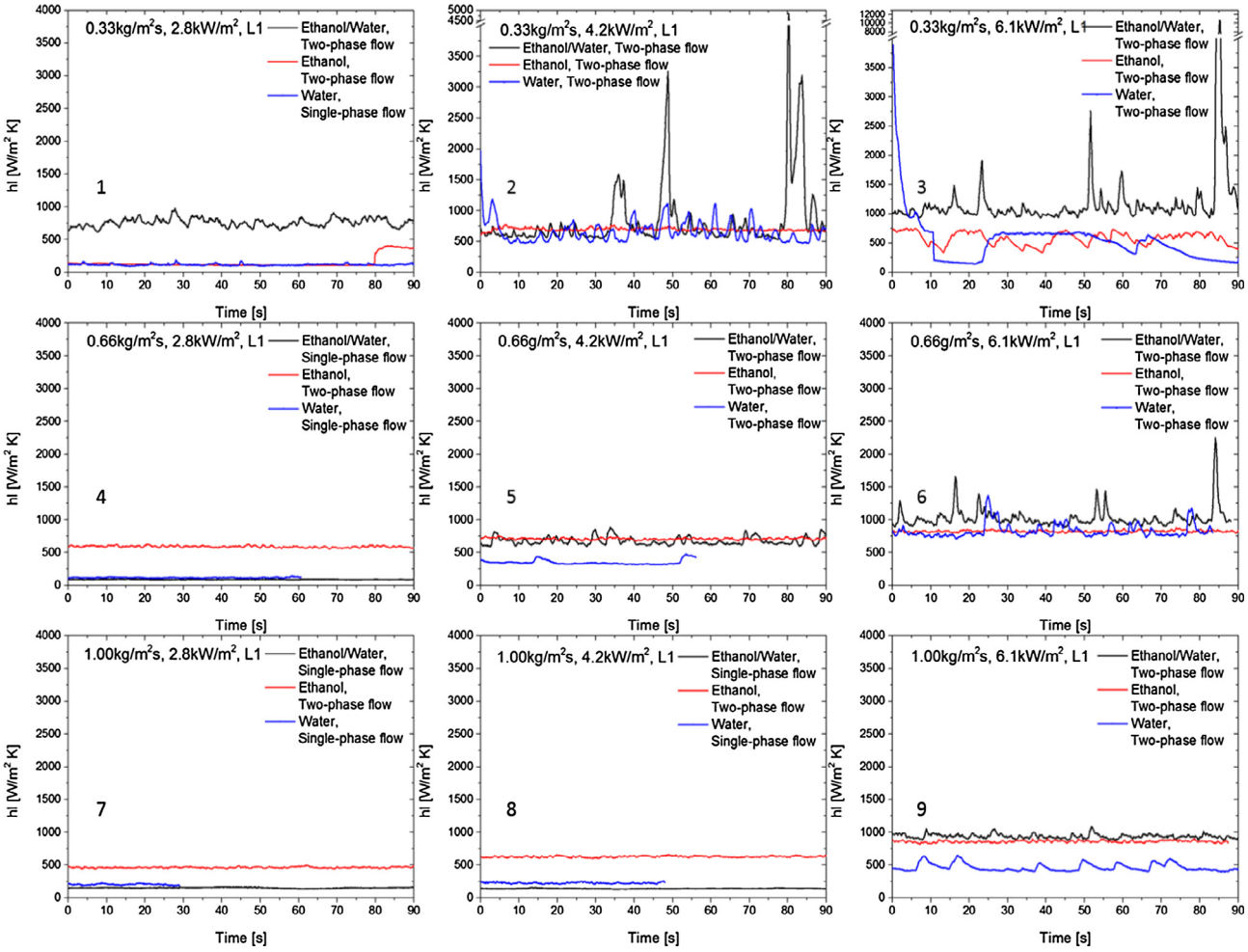

Fig. 11. Local heat transfer coefficient over time of 5% v/v ethanol/water mixture, water and ethanol for: G = 0.33 kg/m^2 s at (1) q = 2.8 kW/m^2, (2) q = 4.2 kW/m^2, (3) q = 6.1 kW/m^2, G = 0.66 kg/m^2 s at (4) q = 2.8 kW/m^2, (5) q = 4.2 kW/m^2, (6) q = 6.1 kW/m^2, G = 1.00 kg/m^2 s at (7) q = 2.8 kW/m^2, (8) q = 4.2 kW/m^2, (9) q = 6.1 kW/m^2.

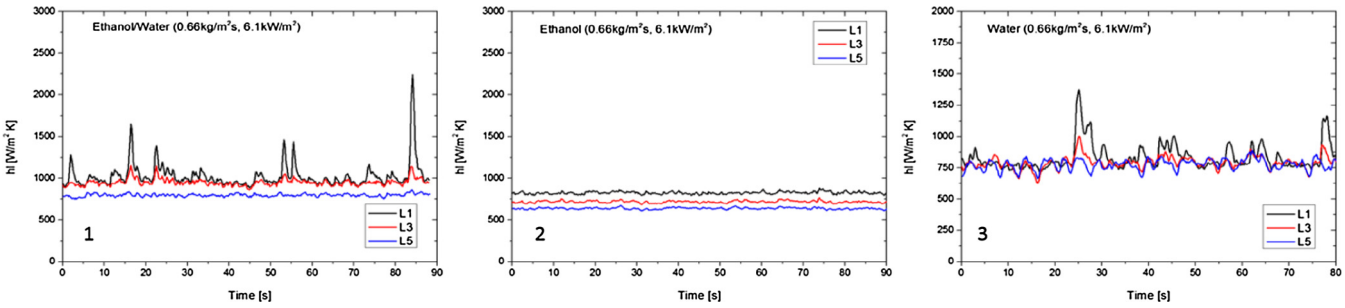

Fig. 12. Local heat transfer coefficient over time of 5% v/v ethanol/water mixture, water and ethanol at G = 0.66 kg/m^2 s and q = 6.1 kW/m^2 for (1) ethanol/water (2) ethanol and (3) water.

especially for water, at the two lower heat fluxes (2.8 and 4.2 kW/m^2), due to single phase flow prevailing. At the highest heat flux (6.1 kW/m^2), the increase of mass flux only appeared to have a significant effect on the heat transfer coefficients for pure water, having a lesser effect on pure ethanol or on the ethanol/water mixture. However, for the lower mass fluxes, there were greater fluctuations in the heat transfer coefficient, especially for the ethanol water mixture, with significant periods of very high heat transfer. Examining the calculated local heat transfer coefficients in synchronisation with the high speed imaging, it was observed that higher h_L values were obtained when slug/annular flow was present in the channel, as opposed to bubble flow being present. It could thus be suggested that in these cases another heat transfer mechanism was activated, such as liquid film evaporation working along with forced convection.

Temporally averaged local heat transfer coefficients were also calculated to allow for a numerical comparison between the different fluids. These average local heat transfer coefficients at the lowest mass flux and highest heat flux (0.33 kg/m^2 s and 6.1 kW/m^2) at position L1 are: 420 W/m^2 K for ethanol, 540 W/m^2 K for water and 1200 W/m^2 K for the ethanol/water mixture (three times higher than that of ethanol and roughly twice as high as that of water). However, in the case of both the highest mass and heat flux (1.00 kg/m^2 s and 6.1 kW/m^2), the ethanol and the ethanol/water mixture h_L values were closer together, 940 W/m^2 K for ethanol/water and 860 W/m^2 K for ethanol, while the value of the water heat transfer coefficient was substantially lower (460 W/m^2 K). Principally, the heat transfer coefficients values for the fluids were closer together when mass flux was increased and, given the uncertainty of the calculated values (±20%), it was not possible to distinguish which fluid was more efficient for heat transfer at higher mass fluxes.

A temporal comparison of the heat transfer coefficients for each fluid with position (L1, L3 and L5) for the intermediate mass flux and highest heat flux is provided in Fig. 12. It can be seen that the highest local heat transfer coefficients occur near the channel exit (position L1), which is to be expected since the fluids enter subcooled.

For both the ethanol/water mixture and pure water there are significant fluctuations in the heat transfer coefficient, especially near the exit of the channel. This is linked to the passage of slugs of vapour through the channel. For pure ethanol, the heat transfer coefficients remain fairly constant with time, though they increase with position towards the exit of the channel. For the ethanol/water mixture, boiling/evaporation occurs at different rates for each component (more volatile component evaporates first) leading to a concentration gradient. Thus Marangoni forces can be induced affecting the movement of bulk liquid towards the contact line [13]. It would appear that this behaviour results in a better liquid distribution in the channel, which in turn helps prevent dry-out from happening, and allows higher heat transfer coefficients to be achieved.

5. Conclusions

In this study, two-phase flow heat transfer for a 5% v/v ethanol/water mixture and its pure components (water and ethanol) was investigated. High speed images of the boiling process were obtained, along with the channel wall temperature and the pressure drop across the channel. These were used to calculate local heat transfer coefficients.

Several boiling patterns were identified, that were common for all the fluids, but varied depending on the operating conditions used in each experiment. The boiling regimes observed were: bubble, slug and elongated slug/annular flow.

The channel wall temperature was recorded over time and analysed to determine the effect boiling had on it, and more specifically, how different boiling regimes influenced its fluctuations. It was concluded that channel wall temperature fluctuated over time with two-phase flow, and that this was solely a result of boiling occurring in the channel. It was seen that for the ethanol/water mixture, the amplitude of the fluctuations was significantly lower than for the pure liquids, allowing for a more stable heat transfer process over time.

Thus the heat transfer in the test section was found to have been enhanced by the addition of a small amount of ethanol into water (5% v/v ethanol/water mixture), resulting in higher heat transfer coefficients than both of its pure components. The temporal variation in heat transfer coefficients were found from high speed imaging to correlate with vapour slug formation and expulsion from the channel. From the lower wall temperature fluctuations it is clear that the use of the mixture can help to ensure the prevention of a wall dry-out, which could lead in a potential critical failure in a cooling system.

Acknowledgements

This research was supported by the UK Engineering and Physical Sciences Research Council (EPSRC) grant EP/N011341/1.

References

[1] Y.Y. Yan, T.F. Lin, Condensation heat transfer and pressure drop of refrigerant R-134a in a small pipe, Int. J. Heat Mass Transf. 42 (4) (1999) 697–708.
[2] S. Lin, K. Sefiane, J.R.E. Christy, Prospects of confined flow boiling in thermal management of microsystems, Appl. Therm. Eng. 22 (2002) 825–837.
[3] Y. Gan, J. Xu, S. Wang, Are the available boiling heat transfer coefficients suitable for silicon microchannel heat sinks?, Microfluid Nanofluid 4 (2008) 575–587
[4] T.N. Tran, M.W. Wambsganss, D.M. France, Small circular- and rectangular-channel boiling with two refrigerants, Int. J. Multiph. Flow 22 (3) (1996) 485–498.
[5] J.R. Thome, State-of-the-Art Overview of Boiling and Two-Phase Flows in Microchannels, Heat Transf. Eng. 27 (9) (2006) 4–19.
[6] X.F. Peng, H.Y. Hu, B.X. Wang, Boiling nucleation during liquid flow in microchannels, Int. J. Heat Mass Transf. 41 (l) (1998) 101–106.

[7] A. Greco, G.P. Vanoli, Flow boiling heat transfer with HFC mixtures in a smooth horizontal tube. Part I: Experimental investigations, Exp. Therm. Fluid Sci. 29 (2) (2005) 189–198.
[8] A. Kaya, M.R. Özdemir, A. Koşar, High mass flux flow boiling and critical heat flux in microscale, Int. J. Therm. Sci. 65 (2013) 70–78.
[9] W. Yu, D.M. France, M.W. Wambsganss, J.R. Hull, Two-phase pressure drop, boiling heat transfer, and critical heat flux to water in a small-diameter horizontal tube, Int. J. Multiph. Flow 28 (6) (2002) 927–941.
[10] A. Koşar, C.J. Kuo, Y. Peles, Boiling heat transfer in rectangular microchannels with reentrant cavities, Int. J. Heat Mass Transf. 48 (23–24) (2005) 4867–4886.
[11] B. Sumith, F. Kaminaga, K. Matsumura, Saturated flow boiling of water in a vertical small diameter tube, Exp. Therm. Fluid Sci. 27 (7) (Sep. 2003) 789–801.
[12] W.R. Mcgillis, J.S. Fitch, W.R. Hamburgen, V.P. Carey, WRL technical note TN-23 boiling binary mixtures at subatmospheric pressures, 1999.
[13] B.R. Fu, M.S. Tsou, C. Pan, Boiling heat transfer and critical heat flux of ethanol-water mixtures flowing through a diverging microchannel with artificial cavities, Int. J. Heat Mass Transf. 55 (5–6) (2012) 1807–1814.
[14] K. Suzuki, T. Kokubu, M. Nakano, H. Kawamura, I. Ueno, H. Shida, O. Ogawa, Enhancement of heat transfer in subcooled flow boiling with microbubble emission, Exp. Therm. Fluid Sci. 29 (7 SPEC. ISS.) (2005) 827–832.
[15] R.K. Shah, A.L. London, Laminar Flow Forced Convection in Ducts: A Source Book for Compact Heat Exchanger Analytical Data, Academic Press, 2014.
[16] C. Huh, M.H. Kim, Pressure drop, boiling heat transfer and flow patterns during flow boiling in a single microchannel, Heat Transf. Eng. 28 (8–9) (2007) 730–737.
[17] K. Mishima, T. Hibiki, Some characteristics of air-water two-phase flow in small diameter vertical tubes, Int. J. Multiph. Flow 22 (4) (1996) 703–712.
[18] V.P. Carey, Heterogeneous Nucleation and Bubble Growth in Liquids. Liquid-Vapor Phase-Change Phenomena: An Introduction to the Thermophysics of Vaporization and Condensation Processes in Heat Transfer Equipment, Taylor & Francis, 2008.
[19] S.S. Bertsch, E.A. Groll, S.V. Garimella, Effects of heat flux, mass flux, vapor quality, and saturation temperature on flow boiling heat transfer in microchannels, Int. J. Multiph. Flow 35 (2) (2009) 142–154.